Title

A Designed Inhibitor of p53 Aggregation Rescues p53 Tumor Suppression in Ovarian Carcinomas

Journal

Cancer Cell, 29(1)

ISSN

1535-6108

Authors

Soragni, Alice

Janzen, Deanna M

Johnson, Lisa M

et al.

Publication Date

2016

DOI

10.1016/j.ccell.2015.12.002

Peer reviewed

HHS Public Access

Author manuscript

Cancer Cell. Author manuscript; available in PMC 2017 January 11.

Published in final edited form as:

Cancer Cell. 2016 January 11; 29(1): 90–103. doi:10.1016/j.ccell.2015.12.002.

A designed inhibitor of p53 aggregation rescues p53 tumor-suppression in ovarian carcinomas

Alice Soragni[1], **Deanna M. Janzen**[2], **Lisa M. Johnson**[1], **Anne G. Lindgren**[2], **Anh Thai-Quynh Nguyen**[1,‡], **Ekaterina Tiourin**[2], **Angela B. Soriaga**[1], **Jing Lu**[3], **Lin Jiang**[1,§], **Kym F. Faull**[4], **Matteo Pellegrini**[3], **Sanaz Memarzadeh**[2,5,6,7,*], and **David S. Eisenberg**[1,7,*]

[1]UCLA-DOE Institute, HHMI, and Departments of Biological Chemistry and Chemistry and Biochemistry, 611 S. Charles E. Young Dr., Los Angeles, CA 90095-1570, USA

[2]Department of Obstetrics and Gynecology, David Geffen School of Medicine, University of California Los Angles, Los Angeles, CA 90095

[3]Molecular, Cell and Developmental Biology, University of California Los Angles, Los Angeles, CA 90095

[4]Pasarow Mass Spectrometry Laboratory, Semel Institute, 405 Hilgard Avenue, Los Angeles CA 90095

[5]Eli and Edythe Broad Center of Regenerative Medicine and Stem Cell Research, University of California Los Angles, Los Angeles, CA 90095

[6]The VA Greater Los Angeles Health Care System, Los Angeles, CA, 90073

SUMMARY

Half of all human cancers lose p53 function by missense mutations, with an unknown fraction of these containing p53 in a self-aggregated, amyloid-like state. Here we show that a cell-penetrating peptide, ReACp53, designed to inhibit p53 amyloid formation, rescues p53 function in cancer cell lines and in organoids derived from high-grade serous ovarian carcinomas (HGSOC), an aggressive cancer characterized by ubiquitous p53 mutations. Rescued p53 behaves similarly to its wild-type counterpart in regulating target genes, reducing cell proliferation and increasing cell death. Intraperitoneal administration decreases tumor proliferation and shrinks xenografts *in vivo*. Our data show the effectiveness of targeting a specific aggregation defect of p53 and its potential applicability to HGSOCs.

[*]Correspondence to S.M. (smemarzadeh@mednet.ucla.edu) and D.S.E. (david@mbi.ucla.edu).

[7]Co-senior authors

[‡]Present address: Laboratory of Stem Cell Research and Application, University of Science, Vietnam National University, HCM City, Vietnam

[§]Present address: Department of Neurology, Mary S. Easton Center for Alzheimer's Disease Research, David Geffen School of Medicine, University of California at Los Angeles, Los Angeles, California 90095, United States

INTRODUCTION

p53 is a tumor suppressor of paramount importance and the most frequently mutated protein in human cancers (Lane and Crawford, 1979; Levine and Oren, 2009; Linzer and Levine, 1979). It arrests proliferation and promotes either DNA repair or apoptosis in cells with DNA damage or under stresses such as hypoxia or starvation (Vazquez et al. 2008; Vousden and Ryan, 2009). In over half of all tumors p53 is inactivated by a single point mutation, most frequently in the DNA binding domain. These mutations inactivate the protein, either by altering a residue which directly contacts DNA (contact mutants) or by mutating a residue which destabilizes and partially unfolds p53 (structural mutants), although the separation between classes is not absolute (Joerger and Fersht, 2008).

Depending on cancer type the percentage of cases bearing p53 mutations varies. One of the subtypes presenting with the highest prevalence are high-grade serous ovarian carcinomas (HGSOC), where mutations are reported in >96% of cases (TCGA, 2011; Ahmed et al., 2010). Ovarian cancer is the most lethal of all gynecologic cancers and the fifth most common cause of cancer-related death among women in the US (Siegel et al., 2014). About 80% of all ovarian cancers are of the serous type, mostly diagnosed at advanced stages with poor long-term prognosis (Seidman et al., 2004). Despite surgical debulking and administration of platinum-based chemotherapy, almost all patients suffer from recurrent and disseminated disease and the majority dies in less than 5 years (Vaughan et al., 2011). Efforts aimed at developing new therapeutic approaches have largely been unsuccessful. An early event in carcinogenesis, p53 inactivation through mutation is associated with poor response to treatment and poor prognosis (Kurman et al., 2008; Leitao et al., 2004). Although p53 alterations are so prevalent in ovarian cancer, there is as of yet no targeted therapy approved for restoring p53 function.

Over the past decade, p53 and fragments thereof have been shown to aggregate *in vitro* (Silva et al., 2014). More recently, several p53 mutants were found as amyloid aggregates in tumor cell lines (Xu et al., 2011) and breast cancer biopsies (Levy et al., 2011). These aggregates inactivate p53 by sequestering the protein, thus blocking its transcriptional activity and pro-apoptotic function (Xu et al., 2011).

Our working hypothesis based on the behavior of other amyloid-forming proteins (Eisenberg and Jucker, 2012), is that each aggregation-promoting mutation initially destabilizes the native protein structure causing exposure of an adhesive sequence (Wang and Fersht, 2012). This segment binds to segments alike from other p53 molecules, resulting in protein aggregation and inactivation. The following questions related to p53 aggregation are presently unanswered: (1) Can inhibition of p53 aggregation in these cells rescue normal p53 function? (2) Does such reactivation halt cell proliferation and diminish tumor size *in vivo*? (3) Does reactivation of p53 avoid on-target toxicities in normal tissues?

Here we address these questions by designing a cell permeable 17-residue peptide inhibitor of p53 aggregation. Reflecting the intended function of this inhibitor as a rescuer of the activity of p53, we call it ReACp53.

RESULTS

p53 amyloid spine structure and its use to design a sequence-specific aggregation inhibitor

Several segments in the DNA binding domain of p53 are prone to form an amyloid adhesive segment, termed a steric zipper, as calculated by the ZipperDB algorithm which identified residues 252-258 as the most aggregation-prone in this region (Figure 1A, Goldschmidt et al., 2010). The segment 251-257 has been reported as necessary and sufficient to drive p53 aggregation in cell lines (Ghosh et al., 2014; Xu et al., 2011). We focused on the two partially overlapping segments 252-LTIITLE-258 and 253-TIITLE-258, and chemically synthesized them. Both formed amyloid-like fibrils and microcrystals that enabled their structure determination at atomic resolution (Sawaya et al., 2007; Figure S1 and Table S1). The segments aggregated as tight, dry steric zippers, with LTIITLE forming a class 2, face-to-back amyloid spine while TIITLE formed a class 1, face-to-face interface. Since both shared similar side-chain contacts, we were able to design an inhibitor that can interact with both and block further aggregation.

Next, we implemented a modified rational approach to design a peptidic inhibitor starting from the LTIITLE structure (Sievers et al., 2011). In order to maximize sequence specificity and avoid off-target effects, we kept the original p53 sequence, but included single or double aggregation-inhibiting residues such as K or R (Ghosh et al., 2014; Härd and Lendel, 2012) in critical positions as judged by the side chain arrangement in the LTIITLE structure we determined. Various residues were replaced in position 1, 3 and 5 (Table S2), and segments were computationally analyzed with Rosetta to score their structural complementarity to the original template (Leaver-Fay et al., 2011). Candidate peptides were screened for their ability to inhibit aggregation of the target sequence *in vitro* and for specificity, and the best candidate, having sequence LTRITLE, was selected for further studies. When mapped onto the atomic structure of the LTIITLE segment, the arginine substitution in position 3 clashes with the binding of additional LTIITLE molecules (Figure 1C). Experiments confirmed that LTRITLE efficiently blocks peptide aggregation *in vitro* (Figure S1G), with marked effects at substoichiometric concentrations. Although full-length p53 harboring the I254R mutation does not aggregate in cells (Xu et al., 2011), there is no guarantee that an exogenously administered LTRITLE peptide may work as an efficient inhibitor so we proceeded to test this hypothesis. We fused the peptide to an N-terminal poly-arginine cell-penetrating tag (R=9; Fuchs and Raines, 2005), followed by a three residue linker derived from the p53 sequence (RPI) and tested this candidate, ReACp53, in cells.

ReACp53 penetrates into HGSOC primary cancer cells and converts mutant p53 from a punctate state into soluble WT-like p53

We isolated primary cells from a cohort of HGSOC patients (n=7, Table S3) bearing various p53 mutations. We confirmed that ReACp53 could enter the cells by chemically coupling it to a fluorescent FITC moiety. Cells treated with 10 μM FITC-labeled peptide for 16–20h in serum free media showed intracellular and intranuclear staining, indicative of ReACp53 penetration (Figure 2A and S2A–B and E).

When primary cells grown on coverslips were stained for p53, all patient samples harboring the R248Q mutation exhibited cytosolic, punctate staining with little nuclear p53 (Figure 2A–B and S2A). This suggests that in these clinical samples grown as monolayers mutant p53 mostly self-associates in the cytosol. Upon 16–20h of ReACp53 treatment, the proportion of cells with p53 puncta was reduced to 5–20%, and p53 could now be detected in the nucleus in 70 to 100% of cells, depending on the patient (Figure 2A–B). The absence of aggregated cytosolic p53 together with the shift in localization suggests that p53 was disaggregated and possibly restored to a functional form. We confirmed this by staining a stable cell line we established from HGSOC Patient 1 (called S1 GODL; Janzen et al, 2015) with either DO-1 or PAb240 anti-p53 antibodies in the presence of increasing concentrations of ReACp53. DO-1 recognizes any p53, regardless of conformation, while PAb240 is specific for partially unfolded p53. Because partially unfolded p53 is required for protein aggregation, we used PAb240 as a surrogate marker for aggregated p53. As visible in Figure 2C–D, there is less PAb240 binding upon ReACp53 treatment, despite the presence of p53 in the cells as indicated by DO-1 staining, while the scrambled peptide control did not have any effect (Figure S2C). Immunoprecipitation with PAb240 using native lysates from vehicle or ReACp53-treated S1 GODL cells gave analogous results (Figure S2D) Collectively, these data indicate that the antigen recognized by PAb240 (residues 213-217, Figure 1B) is now buried in the protein core and no longer accessible.

ReACp53 induces cancer cell death, cell cycle arrest and results in p53 degradation

Next, we evaluated the effects of ReACp53 on cell viability using OVCAR3 and S1 GODL cells. ReACp53 reduced cell viability in a concentration-dependent manner, while a control sequence-scrambled ReACp53 or the poly-arginine tag alone was ineffective (Figure 3A–B and S3A). The peptide was also effective in the presence of increasing concentrations of serum (Figure 3A), albeit with lower EC_{50} values. Consecutive daily treatments lowered the EC_{50}s even in presence of as much as 10% serum (Figure S3B).

By light microscopy and TEM (Figure S3C–D), mixed features of apoptotic/necrotic cell death were visible, such as nuclear envelope enlargements, isolated nuclear bodies and condensed chromatin. As visible in Figure 3C, ReACp53 increased the proportion of YO-PRO-1 (staining apoptotic cells) and propidium iodide (PI, staining late apoptotic/necrotic cells) OVCAR3-positive cells in a concentration-dependent manner, but a scrambled control peptide did not, strengthening the evidence for sequence specificity of ReACp53. Similar results were obtained in S1 GODL cells (Figure 3D and S3E, quantified by flow cytometry). We could detect Bad cleavage upon 16h ReACp53 treatment at concentrations of 5 μM and above in S1 GODL cells (Figure 3E), indicative of apoptosis. However, the pan-caspase inhibitor QV-OPh only partially rescued cell viability. NEC-1, an inhibitor of necroptosis, similarly showed a significant but incomplete rescue of cell viability (Figure 3F).

Another indication of rescued p53 activity is induction of G0/G1 cell cycle arrest. To test this, we treated S1 GODL cells for 4/5 hours with ReACp53 or a scrambled peptide and examined DNA content by flow cytometry. We detected a small but significant shift in the cell cycle distribution of the asynchronous population, with more cells in G0/G1 and fewer in G2/M phase (Figure 3G). We observed a ~40% reduction in phopsho-Rb(S608/611)

consistent with a G0/G1 cell cycle arrest in progress (Figure S3F–G). Levels of phospho-Chk2 were unaltered upon ReACp53, suggesting that ReACp53 does not induce DNA damage (Figure S3H).

Lastly, we checked for p53 levels upon ReACp53 treatment. p53 cellular levels are tightly controlled to express little protein in the absence of a stimulus (Levine and Oren, 2009). This is due, at least in part, to MDM2, an ubiquitin ligase that targets p53 for proteosomal degradation. Partially unfolded p53 mutants typically cannot interact with MDM2 resulting in protein accumulation (Joerger and Fersht, 2008). In agreement with this hypothesis, we detected high levels of R248Q p53 in S1 GODL cells grown as a monolayer (Figure S3I). Upon ReACp53 treatment, p53 levels gradually decreased. Given that there is less aggregated p53 upon ReACp53 treatment (Figure 2D), we hypothesized that the WT-like folded protein could be interacting with MDM2. We used a pharmacologic approach to test this, by applying Nutlin-3, a p53-MDM2 interaction inhibitor, to S1 GODL cells treated with ReACp53 (Vassilev et al., 2004). Upon combined ReACp53/Nutlin-3 treatment, p53 levels were higher, supporting the idea that the now properly folded mutant p53 can interact with MDM2 (Figure S3J–K). Concurrent treatment with both molecules resulted in a synergistic reduction of EC_{50} values upon addition of 10 μM Nutlin-3 in low passaged S1 GODL cells (Figure S3D–F).

ReACp53 induces rapid cell death in human primary uterine fibroblasts transfected with a dominant negative R175H p53 mutant grown in 3D

To further validate p53 as the primary target of ReACp53 action, we tested its effects on an isogenic background by infecting human primary uterine fibroblasts (UtFIB) with a GFP construct or a GFP/R175H p53-expressing construct (Figure 3H). GFP-positive fibroblasts were sorted and p53 expression was tested by western blot and immunofluorescence (Figure 3I–K). The GFP/R175H p53 expressing UtFIB rapidly changed morphology and started proliferating faster than the GFP control (Figure 3I). In order to study the effects of ReACp53 in a more physiological model system that better recapitulates drug responses observed *in vivo*, we tested UtFIB response to ReACp53 using a 3D Matrigel culture system (L'Espérance et al., 2008). After seeding the cells in Matrigel and allowing them to grow for two days, GFP and GFP/R175H p53 UtFIB were treated twice with increasing ReACp53 concentrations (0–10 μM) and cell death was assessed by Annexin V/PI staining upon release from Matrigel (Figure 3L). The response to ReACp53 in UtFIBs carrying the aggregating R175H p53 mutant was 2 to 10 fold higher than controls.

ReACp53 Acts to Stabilize Mutant p53 *In Vitro*

Consistent with mutant p53 overexpression, we detected significant amount of SDS-resistant p53 high molecular weight aggregates in GFP/R175H UtFIB (Figure S3O). We tested the effects of ReACp53 on p53 stability by adding it to cell lysates of either normal untrasfected UtFIB, GFP/R175H UtFIB or S1 GODL (R248Q p53) lysates, followed by heating at 42°C for 10 minutes. This resulted in a high proportion of mutant p53 SDS-insoluble aggregates, which were significantly reduced by co-incubation with ReACp53 (Figure S3O), indicative of a direct effect of ReACp53 on p53 stability *in vitro*.

ReACp53 specifically affects cell viability and proliferation of cancer cells bearing mutant p53 but not wild type when grown as organoids

We established model organoids by growing S1 GODL cells for two days followed by two consecutive treatments with ReACp53 (Figure 4A). We observed a reduction in cell viability reflected in the increased YO-PRO-1/PI staining (Figure 4B). Typically, S1 GODL organoids are 30–200 μm in diameter, with central cavities filled with vesicles and pili (Figure S4A–C). Organoids treated for two days with 10 μM ReACp53 lose their morphology, with several cells being apoptotic/necrotic (Figure 4C and S4D–J). By TEM, we detected enlarged nuclear envelopes and ER, chromatin condensation and condensed mitochondria (Figure 4D and S4H–J), compatible with late apoptotic/necrotic cell death. Cell death was confirmed by Annexin V/PI staining of organoid cells derived from a panel of control cell lines (MCF7, SKOV3, Detroit562, S1 GODL, Table S4) and clinical samples from 8 patients with different p53 status (Table S3) treated twice with ReACp53. Results show extensive cell death in organoids bearing p53 aggregating mutations, but not WT or null cells (Figure 4E and S4K–M). Longer treatments (one week), resulted in a higher proportion of HGSOC patient-derived organoids undergoing extensive cell death, with apparent EC_{50} values in the low micromolar range (Figure 4F and S4N–O). This was accompanied by a marked reduction in the number of Ki67 proliferating cells (Figure 4G). These results suggest that, in this clinically relevant model, ReACp53 is effective on tumor cells bearing aggregation-prone p53 but not on WT folded protein or cells not expressing p53.

Transcriptional reactivation of p53 by ReACp53

The change in p53 protein conformation and localization, increased cell death, and reduction in proliferation are all compatible with rescued p53 function by ReACp53. To gain further insights, we performed RNAseq of organoids generated from OVCAR3 cells and HGSOC Patient 1 primary cells as well as MCF7 and primary cells derived from an ovarian endometrioid cancer patient (WT p53, Patient 8) as controls, all treated for 2 days with 5 μM ReACp53 (Figure 5A). At a cutoff p-value<0.01, over 2400 transcripts were found to be differentially regulated 1.5 fold or more upon ReACp53 treatment in the OVCAR3 sample, and over 700 for the HGSOC primary sample, with close to 80% overlap between datasets (Figure 5A). The definite differences upon ReACp53 treatment in the two mutant p53 specimens resulted in segregation of treated and untreated samples in an unsupervised clustering. On the other hand, there were few differences in the control samples, so that treated and untreated were randomly clustered (Figure S5A). When examining the adjusted p-value distribution, we found few transcripts with significant p-values in the samples bearing WT p53 (Figure S5B). This suggests that ReACp53 in the conditions tested does not have a significant effect on organoids generated from cells expressing WT p53, neither the cell line (MCF7) nor the primary endometrioid tumor from Patient 8, while eliciting a clear effect at the transcriptional level for cells carrying the aggregating R248Q mutation.

Ingenuity Pathway Analysis (IPA) revealed that the majority of differentially regulated transcripts were related to cellular growth and proliferation, movement, death and survival and cellular development for both OVCAR3 and HGSOC Patient #1 samples (Figure 5B and S6C). Gene Ontology analysis of the OVCAR3 dataset highlighted that the most represented

terms in the upregulated mRNAs were regulation of transcription and RNA metabolic processes, regulation of cell proliferation and cell death, while the downregulated mRNAs were related to oxidation reduction, response to organic substance and cell adhesion, and generation of metabolites and energy (Figure S5D). Upstream regulator analysis of the OVCAR3 dataset performed by IPA revealed how p53 was the most significant upstream transcriptional regulator (Table S5), strengthening the idea that ReACp53 acts on p53. We selected ~80 transcripts which are known either as p53 transcriptional targets or as part of the p53 signaling network and mapped their expression levels for vehicle and ReACp53-treated organoids (Figure 5C and S5E). Among the upregulated mRNAs are some well-characterized p53 targets such as p21, GADD45B, PUMA, NOXA and DRAM1. Significant fold changes for these were found in the responsive tumor sample and OVCAR3 cells only (Figure 5D). Two p53 homologs, p63 and p73, were differentially regulated, with p63 being upregulated and p73 being downregulated also at the protein level in both OVCAR and S1 GODL cells (Figure 5D–F). Beside the p53 network, we identified several metabolic processes that are affected by ReACp53. Among these, glycolysis and gluconeogenesis, citrate cycle, pyruvate, lipids and nicotinamide metabolism and the mevalonate pathway were downregulated (Figure S5F). The latter is of particular interest given that it has been shown to be upregulated by mutant p53 (Freed-Pastor et al., 2012).

ReACp53 detection and pharmacokinetics profile in serum of treated animals

Next we checked *in vivo* stability and resistance to proteolytic cleavage, which are potential challenges for ReACp53 administration. To do so, we determined the *in vivo* pharmacokinetics profile of ReACp53. Given that ReACp53 is a peptide, its unambiguous detection in complex mixtures such as serum required the optimization of a sensitive liquid chromatographic/tandem mass spectrometric assay called multiple reaction monitoring (MRM, see Supplemental Experimental Procedures for details) (Anderson and Hunter, 2006). The assay allowed us to discriminate ReACp53 with high specificity both in serum and tissues.

ReACp53 administered intraperitoneally quickly entered systemic circulation and could be detected in serum of treated mice with a peak concentration of 1.2±0.3 μM at the 1h time point (Fig. S6A–C). Additionally, we could detect ReACp53 in tumor tissue (Figure S6D). While the apparent half-life in serum was ~1.45h, close to 20% of the ReACp53 serum peak concentration was still present in circulation after 24 hours, though we cannot unambiguously determine whether the peptide detected was intact or partially proteolyzed due to the trypsin treatment which is part of the sample preparation procedures (see Supplemental Experimental Procedures). Nevertheless, the high stability of ReACp53 warranted further *in vivo* testing.

In vivo administration of ReACp53 results in reduced tumor proliferation and shrinkage in two HGSOC xenograft models

In the minimal residual disease model, three cohorts of mice (n=3) were injected with a matrigel/OVCAR3 (p53 mutant) suspension on one flank and with a matrigel/MCF7 (WT p53) suspension on the other flank in order to provide an internal control for specificity of ReACp53 to preferentially target mutated aggregation-prone p53. Treatment was started the

same day (Figure 6A). In the treatment protocol, tumors were allowed to develop for two weeks prior to treatment initiation (Figure 6A). In both models, the treatment phase consisted of three weeks of daily intraperitoneal (IP) injections with 15 mg/kg of ReACp53, sequence-scrambled control peptide or vehicle alone. The intraperitoneal route was chosen as IP administration of chemotherapeutic drugs in ovarian cancer patients has been shown to be more efficacious than systemic administration and has been recommended by the National Cancer Institute for existing standard treatments (Morgan et al., 2013). For both models, tumor volumes monitored daily indicated that only OVCAR3 xenografts treated with ReACp53 shrank while both vehicle and scrambled control treated tumors more than doubled in size (Figure 6B–C). Only mutant p53-bearing tumors in the ReACp53-treated mice cohorts were 80–90% smaller in weight than the control cohort (Figure 6B–C), confirming the ability of ReACp53 to limit tumor proliferation and shrink tumors *in vivo*. Analysis of residual tumors from the treatment model by hematoxylin and eosin (H&E) stain showed a higher ratio of matrigel to tumor cells for ReACp53 treated xenografts (Figure 6D). Tumor sections were stained with PanK (marking tumor epithelia), p53 and Ki67 (Figure 6D). A significant reduction of Ki67 positive cells was evident in ReACp53-treated OVCAR3 xenografts, indicative of a reduced proliferative index (Figure 6E and S6I–J). MCF7 xenografts carrying WT p53 were not responsive (Figure 6C) indicating that, at least in this experimental design, tumors harboring a functional WT p53 are unaffected by ReACp53. Similar results were observed in the minimal residual disease model (Figure S6G–J). In this paradigm, administration of ReACp53 resulted in a significant increase in p21 and MDM2 transcription in OVCAR3 but not MCF7 xenografts (Figure S6K).

Piknotic nuclei and scarcity of mitotic figures were evident in the residual grafts, suggestive of extensive cell death and reduced proliferation (Figure S6E). We confirmed this in an independent experiment using pre-established xenografts generated from patient-derived stabilized cells (S1 GODL) treated with either vehicle or ReACp53 for 9 days. mRNA levels for a selection of p53 targets including the pro-apoptotic GADD45b and PUMA were increased in the ReACp53-treated grafts (Figure 6F). IHC analysis evidenced a significant increase in Bax protein levels (Figure 6G). In addition, we performed TUNEL assay and observed a significantly increased number of dying cells in the ReACp53 implants (Figure 6H). These results confirm that ReACp53 not only induces proliferative arrest but also cell death in xenografts bearing mutant p53 *in vivo*.

In vivo administration of ReACp53 in a physiological intraperitoneal disseminated disease model causes cell death and reduction of organ implants

To confirm the therapeutic relevance of ReACp53 we shifted toward a more relevant *in vivo* model by injecting 2.5×10^6 HGSOC patient-derived cells (S1 GODL) intraperitoneally. Organ tumor implants and ascites developed over a two-week period and confirmed histologically before initiation of therapy (Figure 7A). Three mice from the vehicle and ReACp53-treated cohorts were sacrificed after four daily IP treatments and ascites were analyzed. Over 80% of cells were Annexin V and/or PI positive in the ReACp53 group (Figure 7B). We also found a significantly increased population in G0/G1 phase (Figure 7C), supporting proliferative arrest upon ReACp53 administration *in vivo*. After the three weeks of daily IP treatments, mice were sacrificed and ascites and organs were analyzed. An

equal small aliquot of cells derived from the IP cavity by peritoneal lavage were plated in quadruplicates. Only the vehicle and scrambled treated cells grew in culture (Figure 7D). Tumor cells from the peritoneal lavage were pelleted, fixed and embedded for histological analysis. This analysis confirmed that the ReACp53-treated mice had very few residual tumor cells in the peritoneal cavity compared to vehicle or scrambled treated controls (Figure 7E). Similarly, organ implants were less frequent and composed of fewer cells in the ReACp53 mice (Figure 7F–G).

ReACp53 is well tolerated *in vivo*

We monitored the treated mice for possible side effects arising from the administration of ReACp53. Complete cell blood counts and ions, total proteins, kidney and liver function were assayed. As visible from Table S6, we did not detect any significant alteration of values upon ReACp53 treatment when compared to vehicle-treated mice. Anatomy of major organs was unaltered, with no difference between ReACp53, vehicle or scrambled peptide-treated samples (Figure S6M). These results suggest that, at the dose studied, ReACp53 is well tolerated and does not induce measurable toxicities.

DISCUSSION

Folded, partially unfolded and aggregated p53 are in equilibrium (Bullock and Fersht, 2001). p53 aggregation is a highly favored process in those instances where a structural mutation destabilizes the molecule permitting exposure of the adhesive segment $p53_{252\text{-}258}$ that is normally buried deep within the protein (Bullock et al., 1997; Bullock and Fersht, 2001; Xu et al., 2011). Previous efforts to rescue p53 function have focused on stabilizing the native fold by chemical modifications or ligand binding, shifting the equilibrium toward the active conformation. This approach has been successful *in vitro* (Bykov et al., 2002; Issaeva et al., 2003; Liu et al., 2013; Wilcken et al., 2012; Yu et al., 2012) with one molecule advancing to the clinical phase (APR-246, Lehmann et al., 2012; Khoo et al., 2014). The purpose of ReACp53 is also to rescue p53 function, but it acts at a different step of the dynamic equilibrium: p53 aggregation. Once exposed, the adhesive segment 252-258 binds to identical segments in other destabilized p53 molecules. ReACp53 is designed to mask this segment, preventing further aggregation and shifting the folding equilibrium towards its functional, WT-like state (Figure 8). Consistent with this mode of action, when HGSOC patient-derived primary cells are treated with ReACp53, neither unfolded nor aggregated p53 are observed. Rather, the aggregation-prone mutant p53 seen in untreated cells in punctate form in the clinical samples examined is dispersed and relocalized to the nucleus.

When culturing tumor cells as organoids in a physiologically relevant 3D system, we observe that ReACp53-rescued p53 behaves similarly to the WT-counterpart by inducing cell death and cell cycle arrest. In the tumor organoids, these effects were observed only in those HGSOC specimens bearing mutant but not WT p53 protein. In further support of the conversion of p53 in treated cells from aggregated to functional states, we observed by RNAseq that several p53 target genes in organoids generated from OVCAR3 cells bearing R248Q p53 are differentially regulated, including upregulation of canonical p53 targets such as PUMA, NOXA, p21, GADD45B, 14-3-3σ. Our data on this particular set of samples are

consistent with the observation that restoring the oncosuppressive function of WT p53 leads to tumor regression (Ventura et al., 2007).

On the other hand, mutant p53 is a bona fide oncogene. It has been shown that some tumor cells expressing gain-of-function mutants of p53 are addicted to its expression (Muller and Vousden, 2013). As such, given that p53 levels decrease upon ReACp53 treatment, some of the effects observed might be linked to removal of a crucial oncogene. This could potentially be mutation and/or context-dependent (Vaughan et al., 2012). In cells where this process is dominant, one could expect Nutlin to antagonize the effects of ReACp53.

Consistent with the loss of the gain-of-function phenotypes exhibited by mutant p53 is the observation that genes known to be upregulated by mutant p53 were downregulated upon ReACp53 exposure. As an example, we found that most genes in the mevalonate pathway were downregulated. This pathway contributes to cell migration and invasion in ovarian cancer (Hashimoto et al., 2005) and is activated through interaction of mutant p53 with SREBP transcription factors (Freed-Pastor et al., 2012). Blocking the mevalonate pathway in HGSOC has been shown to be beneficial, given that compounds such as alendronate, lovastatin, fluvastatin and zoledronic acid reduce tumor burden and the presence of ascites *in vivo* and tumor invasion *in vitro* and *in vivo* (Hashimoto et al., 2005; Knight et al., 2009; Martirosyan et al., 2010).

Beside the mevalonate pathway, several other metabolic processes are impacted by p53 through various mechanisms (Kruiswijk et al., 2015). ReACp53 treatment resulted in lower mRNA levels for enzymes involved in TCA cycle, oxidative phosphorylation, pyruvate and nicotinamide metabolism, glycolysis and gluconeogenesis. This reduction in glycolytic metabolism may result in lower glucose uptake, suggesting the possibility of using FDG-PET to detect early response to ReACp53 *in vivo*.

While several of the effects of ReACp53 at the transcriptional level are in anticipated directions, some variations were unexpected. One might expect p73 mRNA levels to increase upon p53 activation (Vossio et al., 2002), but our RNAseq data showed a reduction, also reflected at the protein level. Relevant to this finding, in over 70% of ovarian cancers p73 is increased at both mRNA and protein levels (Rufini et al., 2011) and its overexpression has been associated with high grade malignancies (Chen et al., 2000). It was reported that p53 inactivation might cause p73 upregulation through E2F (Tophkhane et al., 2012), although other mechanisms such as direct p73 sequestration through co-aggregation are possible (Xu et al., 2011). Nevertheless, p53 reactivation by ReACp53 in our system is accompanied by a reduction in p73 levels, a potential beneficial effect in ovarian cancer. In summary, directionality of some of the changes we observed by RNAseq may be relevant and beneficial to the specific disease setting.

Arresting p53 aberrant self-aggregation could also block its co-aggregation with other proteins which, upon ReACp53 administration, can resume their functions and contribute to the effects seen. In particular, p63 and p73 have been shown to co-aggregate with mutant p53 (Xu et al., 2011). Alternatively, p63 and p73 might be direct ReACp53 targets as they

both have segments with high similarity to the p53 aggregation-prone sequence (Xu et al., 2011). Whether these or other proteins are targeted by ReACp53 remains to be evaluated.

To characterize ReACp53 effects *in vivo*, we tested it on two xenograft models obtaining an 80 to 90% reduction in tumor burden depending on the paradigm. For these experiments, ReACp53 was administered via IP, a standard route of administration of drugs for the HGSOC patient population. Of note, we observed therapeutic efficacy at distant tumor sites *in vivo*. This is consistent with the favorable stability of ReACp53 in serum, as judged by its PK profile. In addition, efficacy was proven in a physiological disseminated disease model that faithfully recapitulates HGSOC characteristics observed in patients, including presence of ascites and implants in distant organs including liver, omentum and spleen (Naora et al, 2005). Standard blood tests and detailed necropsies revealed no tissue damage or blood alterations, supporting the non-toxic behavior of this peptide.

The usefulness of ReACp53 in cancer treatment may be in co-administration with carboplatin. The current standard of care for HGSOC patients entails platinum-based chemotherapy, with superior effects when administered intraperitoneally (Morgan et al., 2013). Carboplatin generates DNA damage that in turns activates the p53 pathway driving cell death, provided that p53 is functional (Siddik et al., 2003). Given that p53 is frequently mutated and not functional in HGSOC, combining an agent that restores p53 functionality such as ReACp53 with carboplatin therapy may be a valuable therapeutic option that warrants further exploration.

ReACp53 may be effective in treating various cancer types. In principle, it could be useful in all tumors where p53 inactivation arises through partial unfolding and aggregation. With thousands of different p53 mutations described (IARC database, http://p53.iarc.fr), we cannot yet anticipate which will respond to ReACp53, other than the well-established aggregation-prone mutations. We showed here that we can target two of the three most common p53 hotspot mutations in HGSOC (R175 and R248), which account for >15% of all ovarian cancer cases (IARC database, http://p53.iarc.fr). An additional feature is that ReACp53 should have no effect on cells with folded, WT p53. We did not observe significant effects of ReACp53 on WT p53 carrying cells in the organoid 3D assays or *in vivo*. However, ReACp53 may also affect tumors bearing WT p53 if the protein is partially unfolded and aggregated. WT p53 has been reported in a mutant-like, aggregated conformation in basal cell carcinoma and hypoxic tumors (Lasagna-Reeves et al., 2013; Rieber and Strasberg-Rieber, 2012) and therefore could potentially be targeted by ReACp53 in specific cases.

In conclusion, the work presented here supports treating susceptible cancers as protein aggregation diseases as an alternative approach to cancer therapy.

EXPERIMENTAL PROCEDURES

Cell lines and clinical samples

This study was approved by the UCLA Office for the Protection of Research Subjects (IRB 10-000727). High-grade serous cancers, obtained from consented patients, were dissociated

to single cells by enzymatic digestion. The S1 GODL cell line was established from primary cells derived from Patient 1's tumor. A detailed procedure on the derivation and characterization of S1 GODL will be described elsewhere (Janzen et al, 2015). Cell lines were obtained from ATCC, maintained in an 8% CO2 incubator at 37°C and used within 15 passages. All the cells used in this study were propagated in the ATCC recommended serum supplemented media and treated in serum free medium (PrEGM, Lonza).

In vitro 3D organoid assay

Single cell suspensions (20'000 cells/well) were plated around the rim of a 24-well cell culture dish in a 1:1.3 mixture of PrEGM media (Lonza CC-3166) and Matrigel (BD Biosciences), and overlaid with 500 μl of PrEGM. Two days after plating, treatment with ReACp53, scramble peptide or vehicle (DMSO) was initiated. Complete medium change was performed daily. Following treatment (day 2 or day 7, depending on the experiment), HGSOC organoids were released from Matrigel by incubation in 1 mg/ml dispase (Invitrogen). Organoids were incubated in warm 0.05% Trypsin-EDTA, then passed through a 20-gauge syringe to yield single cells. Cell viability was determined by manual cell count. Apoptosis and proliferation were determined by FACS analysis (BD LSR II flow cytometer) of cells after staining for AnnexinV and PI exclusion (BD bioscience) and intracellular Ki67 (Vector Laboratories). For each sample, 0.5 μl of AnnexinV-FITC and 2 μl of 50 μg/ml PI diluted in 1x Annexin Binding buffer were added to cells according to manufacturer's instructions. Ki67 was used at 0.5 μl/sample on fixed cells in PBS. For reporting, results were normalized to vehicle treated controls.

Animal experiments

All animal experiments were approved by the UCLA Animal Research Committee and performed under Division of Laboratory Animal Medicine (DLAM) oversight. Immunocompromised NSG mice (Jackson Laboratories: NOD.Cg-*Prkdc*^{scid}*Il2rg*^{tm1Wjl}/SzJ) were housed on a 12-hour light/dark schedule.

Accession numbers

The RCSB Protein Data Bank accession number for the x-ray atomic resolution structures of the p53 amyloid segments 252-258 and 253-258 are 4RP6 and 4RP7 respectively. The NCBI Gene Expression Omnibus accession number to download the RNAseq data is: GSE74550.

Supplementary Material

Refer to Web version on PubMed Central for supplementary material.

Acknowledgments

We thank Dr. Gregory Lawson for assisting with histological examination of tissues and Dr. Jiaoti Huang for sharing the lentiviral GFP/R175H p53 construct; Dr. Stuart Sievers and Jung-Reem Woo for support with the initial p53 structural characterization; Marco Morselli, Arturo Rinaldi and Dr. Ludmilla Rubbi for the help with libraries preparation; Dr. Hans-Uwe Simon for helpful discussions. We acknowledge Austin Quach and Farbod Fazlollahi support with the MRM assay; the Pasarow Mass Spectrometry Laboratory is supported by the NIH grant 1S10RR023718-01A2. This work was supported by grants from the Pardee Foundation (to A.S.), the NIH

(AG-029430 to D.S.E; R01CA183877 to S.M.), the NIH/National Center for Advancing Translational Science UCLA CTSI Grant UL1TR000124 (to A.S. and D.S.E.), the American Cancer Society (RSG-14-217-01-TBG to S.M.), the National Science Foundation (MCB 0958111, to D.S.E.), the Jonsson Cancer Center Foundation/UCLA (to S.M. and D.S.E.); the Lynne Cohen Foundation, the Phase One Foundation, the Ovarian Cancer Circle Inspired by Robin Babbini, the Leath L. and Marcia L. Millen Family Fund and the G.O. Discovery Lab Foundation (to S.M.), the HHMI (to D.S.E.) and in part by a VA CDA-2 award (1 K12 BX 001305-01 to S.M.). A.S., L.J. and D.S.E. are inventors on a patent application based on ReACp53 (WO2014182961 A1). A.S. is a consultant for ADRx, Inc.; D.S.E. is a founder, head of the scientific advisory board and equity holder of ADRx, Inc.

References

Ahmed AA, Etemadmoghadam D, Temple J, Lynch AG, Riad M, Sharma R, Stewart C, Fereday S, Caldas C, Defazio A, et al. Driver mutations in TP53 are ubiquitous in high grade serous carcinoma of the ovary. J Pathol. 2010; 221:49–56. [PubMed: 20229506]

Anderson L, Hunter CL. Quantitative mass spectrometric multiple reaction monitoring assays for major plasma proteins. Mol Cell Proteomics. 2006; 5:573–588. [PubMed: 16332733]

Bullock AN, Fersht AR. Rescuing the function of mutant p53. Nat Rev Cancer. 2001; 1:68–76. [PubMed: 11900253]

Bullock AN, Henckel J, DeDecker BS, Johnson CM, Nikolova PV, Proctor MR, Lane DP, Fersht AR. Thermodynamic stability of wild-type and mutant p53 core domain. Proc Natl Acad Sci USA. 1997; 94:14338–14342. [PubMed: 9405613]

Bykov VJN, Issaeva N, Shilov A, Hultcrantz M, Pugacheva E, Chumakov P, Bergman J, Wiman KG, Selivanova G. Restoration of the tumor suppressor function to mutant p53 by a low-molecular-weight compound. Nat Med. 2002; 8:282–288. [PubMed: 11875500]

Chang SJ, Hodeib M, Chang J, Bristow RE. Survival impact of complete cytoreduction to no gross residual disease for advanced-stage ovarian cancer: a meta-analysis. Gynecol Oncol. 2013; 130:493–498. [PubMed: 23747291]

Chen CL, Ip SM, Cheng D, Wong LC, Ngan HY. P73 gene expression in ovarian cancer tissues and cell lines. Clin Cancer Res. 2000; 6:3910–3915. [PubMed: 11051237]

Eisenberg D, Jucker M. The amyloid state of proteins in human diseases. Cell. 2012; 148:1188–1203. [PubMed: 22424229]

Freed-Pastor WA, Mizuno H, Zhao X, Langerød A, Moon SH, Rodriguez-Barrueco R, Barsotti A, Chicas A, Li W, Polotskaia A, et al. Mutant p53 Disrupts Mammary Tissue Architecture via the Mevalonate Pathway. Cell. 2012; 148:244–258. [PubMed: 22265415]

Fuchs SM, Raines RT. Polyarginine as a multifunctional fusion tag. Protein Sci. 2005; 14:1538–1544. [PubMed: 15930002]

Ghosh S, Ghosh D, Ranganathan S, Anoop A, PSK, Jha NN, Padinhateeri R, Maji SK. Investigating the intrinsic aggregation potential of evolutionarily conserved segments in p53. Biochemistry. 2014; 53:5995–6010. [PubMed: 25181279]

Goldschmidt L, Teng PK, Riek R, Eisenberg D. Identifying the amylome, proteins capable of forming amyloid-like fibrils. Proc Natl Acad Sci USA. 2010; 107:3487–3492. [PubMed: 20133726]

Härd T, Lendel C. Inhibition of Amyloid Formation. Journal of Molecular Biology. 2012; 421:441–465. [PubMed: 22244855]

Hashimoto K, Morishige K, Sawada K, Tahara M, Kawagishi R, Ikebuchi Y, Sakata M, Tasaka K, Murata Y. Alendronate Inhibits Intraperitoneal Dissemination in In vivo Ovarian Cancer Model. Cancer Res. 2005; 65:540–545. [PubMed: 15695397]

Issaeva N, Friedler A, Bozko P, Wiman KG, Fersht AR, Selivanova G. Rescue of mutants of the tumor suppressor p53 in cancer cells by a designed peptide. Proc Natl Acad Sci USA. 2003; 100:13303–13307. [PubMed: 14595027]

Janzen DM, Tiourin E, Salehi JA, Paik DY, Lu J, Pellegrini M, Memarzadeh S. An apoptosis-enhancing drug overcomes platinum resistance in a tumour-initiating subpopulation of ovarian cancer. Nat Commun. 2015; 6

Joerger AC, Fersht AR. Structural Biology of the Tumor Suppressor p53. Annual Review of Biochemistry. 2008; 77:557–582.

Khoo KH, Verma CS, Lane DP. Drugging the p53 pathway: understanding the route to clinical efficacy. Nat Rev Drug Discov. 2014; 13:217–236. [PubMed: 24577402]

Knight LA, Kurbacher CM, Glaysher S, Fernando A, Reichelt R, Dexel S, Reinhold U, Cree IA. Activity of mevalonate pathway inhibitors against breast and ovarian cancers in the ATP-based tumour chemosensitivity assay. BMC Cancer. 2009; 9:38. [PubMed: 19175937]

Kruiswijk F, Labuschagne CF, Vousden KH. p53 in survival, death and metabolic health: a lifeguard with a licence to kill. Nat Rev Mol Cell Biol. 2015; 16:393–405. [PubMed: 26122615]

Kurman RJ, Shih I-M. Pathogenesis of Ovarian Cancer: Lessons From Morphology and Molecular Biology and Their Clinical Implications. International Journal of Gynecological Pathology PAP. 2008

Lane DP, Crawford LV. T antigen is bound to a host protein in SY40-transformed cells. Nature. 1979; 278:261–263. [PubMed: 218111]

Lasagna-Reeves CA, Clos AL, Castillo-Carranza D, Sengupta U, Guerrero-Muñoz M, Kelly B, Wagner R, Kayed R. Dual role of p53 amyloid formation in cancer; loss of function and gain of toxicity. Biochem Biophys Res Commun. 2013; 430:963–968. [PubMed: 23261448]

Leaver-Fay A, Tyka M, Lewis SM, Lange OF, Thompson J, Jacak R, Kaufman K, Renfrew PD, Smith CA, Sheffler W, et al. ROSETTA3: an object-oriented software suite for the simulation and design of macromolecules. Meth Enzymol. 2011; 487:545–574. [PubMed: 21187238]

Lehmann S, Bykov VJN, Ali D, Andrén O, Cherif H, Tidefelt U, Uggla B, Yachnin J, Juliusson G, Moshfegh A, et al. Targeting p53 in vivo: a first-in-human study with p53-targeting compound APR-246 in refractory hematologic malignancies and prostate cancer. J Clin Oncol. 2012; 30:3633–3639. [PubMed: 22965953]

Leitao MM, Soslow RA, Baergen RN, Olvera N, Arroyo C, Boyd J. Mutation and expression of the TP53 gene in early stage epithelial ovarian carcinoma. Gynecol Oncol. 2004; 93:301–306. [PubMed: 15099937]

L'Espérance S, Bachvarova M, Tetu B, Mes-Masson AM, Bachvarov D. Global gene expression analysis of early response to chemotherapy treatment in ovarian cancer spheroids. BMC Genomics. 2008; 9:99. [PubMed: 18302766]

Levine AJ, Oren M. The first 30 years of p53: growing ever more complex. Nat Rev Cancer. 2009; 9:749–758. [PubMed: 19776744]

Levy CB, Stumbo AC, Ano Bom APD, Portari EA, Cordeiro Y, Carneiro Y, Silva JL, De Moura-Gallo CV. Co-localization of mutant p53 and amyloid-like protein aggregates in breast tumors. Int J Biochem Cell Biol. 2011; 43:60–64. [PubMed: 21056685]

Linzer DIH, Levine AJ. Characterization of a 54K Dalton cellular SV40 tumor antigen present in SV40-transformed cells and uninfected embryonal carcinoma cells. Cell. 1979; 17:43–52. [PubMed: 222475]

Liu X, Wilcken R, Joerger AC, Chuckowree IS, Amin J, Spencer J, Fersht AR. Small molecule induced reactivation of mutant p53 in cancer cells. Nucleic Acids Res. 2013; 41:6034–6044. [PubMed: 23630318]

Martirosyan A, Clendening JW, Goard CA, Penn LZ. Lovastatin induces apoptosis of ovarian cancer cells and synergizes with doxorubicin: potential therapeutic relevance. BMC Cancer. 2010; 10:103. [PubMed: 20298590]

Morgan RJ, Alvarez RD, Armstrong DK, Burger RA, Chen L, Copeland L, Crispens MA, Gershenson DM, Gray HJ, Hakam A, et al. Ovarian Cancer, Version 2.2013. J Natl Compr Canc Netw. 2013; 11:1199–1209. [PubMed: 24142821]

Muller PAJ, Vousden KH. p53 mutations in cancer. Nat Cell Biol. 2013; 15:2–8. [PubMed: 23263379]

Network TCGAR. Integrated genomic analyses of ovarian carcinoma. Nature. 2011; 474:609–615. [PubMed: 21720365]

Newton TR, Parsons PG, Lincoln DJ, Cummings MC, Wyld DK, Webb PM, Green AC, Boyle GM. Expression profiling correlates with treatment response in women with advanced serous epithelial ovarian cancer. Int J Cancer. 2006; 119:875–883. [PubMed: 16557592]

Naora H, Montell DJ. Ovarian Cancer Metastasis: Integrating insights from disparate model organisms. Nat Rev Cancer. 2005; 5:355–366. [PubMed: 15864277]

Rieber M, Strasberg-Rieber M. Hypoxia, Mn-SOD and H(2)O(2) regulate p53 reactivation and PRIMA-1 toxicity irrespective of p53 status in human breast cancer cells. Biochem Pharmacol. 2012; 84:1563–1570. [PubMed: 22982566]

Rufini A, Agostini M, Grespi F, Tomasini R, Sayan BS, Niklison-Chirou MV, Conforti F, Velletri T, Mastino A, Mak TW, et al. p73 in Cancer. Genes Cancer. 2011; 2:491–502. [PubMed: 21779517]

Sawaya MR, Sambashivan S, Nelson R, Ivanova MI, Sievers SA, Apostol MI, Thompson MJ, Balbirnie M, Wiltzius JJW, McFarlane HT, et al. Atomic structures of amyloid cross-beta spines reveal varied steric zippers. Nature. 2007; 447:453–457. [PubMed: 17468747]

Seidman JD, Horkayne-Szakaly I, Haiba M, Boice CR, Kurman RJ, Ronnett BM. The histologic type and stage distribution of ovarian carcinomas of surface epithelial origin. Int J Gynecol Pathol. 2004; 23:41–44. [PubMed: 14668549]

Siddik ZH. Cisplatin: mode of cytotoxic action and molecular basis of resistance. Oncogene. 2003; 22:7265–7279. [PubMed: 14576837]

Siegel R, Ma J, Zou Z, Jemal A. Cancer statistics, 2014. CA A Cancer Journal for Clinicians. 2014; 64:9–29. [PubMed: 24399786]

Sievers SA, Karanicolas J, Chang HW, Zhao A, Jiang L, Zirafi O, Stevens JT, Münch J, Baker D, Eisenberg D. Structure-based design of non-natural amino-acid inhibitors of amyloid fibril formation. Nature. 2011; 475:96–100. [PubMed: 21677644]

Silva JL, Gallo CVDM, Costa DCF, Rangel LP. Prion-like aggregation of mutant p53 in cancer. Trends in Biochemical Sciences. 2014; 39:260–267. [PubMed: 24775734]

Tophkhane C, Yang SH, Jiang Y, Ma Z, Subramaniam D, Anant S, Yogosawa S, Sakai T, Liu WG, Edgerton S, et al. p53 inactivation upregulates p73 expression through E2F-1 mediated transcription. PLoS ONE. 2012; 7:e43564. [PubMed: 22952705]

Vassilev LT, Vu BT, Graves B, Carvajal D, Podlaski F, Filipovic Z, Kong N, Kammlott U, Lukacs C, Klein C, et al. In vivo activation of the p53 pathway by small-molecule antagonists of MDM2. Science. 2004; 303:844–848. [PubMed: 14704432]

Vaughan CA, Frum R, Pearsall I, Singh S, Windle B, Yeudall A, Deb SP, Deb S. Allele specific gain-of-function activity of p53 mutants in lung cancer cells. Biochem Biophys Res Commun. 2012; 428:6–10. [PubMed: 22989750]

Vaughan S, Coward JI, Bast RC, Berchuck A, Berek JS, Brenton JD, Coukos G, Crum CC, Drapkin R, Etemadmoghadam D, et al. Rethinking ovarian cancer: recommendations for improving outcomes. Nat Rev Cancer. 2011; 11:719–725. [PubMed: 21941283]

Vazquez A, Bond EE, Levine AJ, Bond GL. The genetics of the p53 pathway, apoptosis and cancer therapy. Nat Rev Drug Discov. 2008; 7:979–987. [PubMed: 19043449]

Ventura A, Kirsch DG, McLaughlin ME, Tuveson DA, Grimm J, Lintault L, Newman J, Reczek EE, Weissleder R, Jacks T. Restoration of p53 function leads to tumour regression in vivo. Nature. 2007; 445:661–665. [PubMed: 17251932]

Vossio S, Palescandolo E, Pediconi N, Moretti F, Balsano C, Levrero M, Costanzo A. DN-p73 is activated after DNA damage in a p53-dependent manner to regulate p53-induced cell cycle arrest. Oncogene. 2002; 21:3796–3803. [PubMed: 12032848]

Vousden KH, Ryan KM. p53 and metabolism. Nat Rev Cancer. 2009; 9:691–700. [PubMed: 19759539]

Wang G, Fersht AR. First-order rate-determining aggregation mechanism of p53 and its implications. Proc Natl Acad Sci USA. 2012; 109:13590–13595. [PubMed: 22869710]

Wilcken R, Wang G, Boeckler FM, Fersht AR. Kinetic mechanism of p53 oncogenic mutant aggregation and its inhibition. Proc Natl Acad Sci USA. 2012; 109:13584–13589. [PubMed: 22869713]

Xu J, Reumers J, Couceiro JR, De Smet F, Gallardo R, Rudyak S, Cornelis A, Rozenski J, Zwolinska A, Marine JC, et al. Gain of function of mutant p53 by coaggregation with multiple tumor suppressors. Nat Chem Biol. 2011; 7:285–295. [PubMed: 21445056]

Yu X, Vazquez A, Levine AJ, Carpizo DR. Allele Specific p53 Mutant Reactivation. Cancer Cell. 2012; 21:614–625. [PubMed: 22624712]

SIGNIFICANCE

Among all cancers, HGSOC has the highest rate of p53 mutations and no curative therapies, so it is an ideal test system for p53-reactivating molecules such as ReACp53. Because aggregation of p53 has been observed in a variety of tumors, ReACp53 can also be applied to other cancers. By inhibiting p53 aggregation, ReACp53, alters the dynamic equilibrium between folded, partially unfolded and aggregated p53, re-instating a pool of functional WT-like protein capable of driving tumor regression. ReACp53 rescues the function of two of the most commonly mutated residues, R175 and R248. While many mutants may aggregate and respond to ReACp53, these two alone are present in tumors of ~80,000 U.S. patients/year, who could potentially benefit from a p53-aggregation inhibition therapy.

Highlights

- We designed the peptide ReACp53 to halt aggregation of p53 in cells
- ReACp53 rescues p53 transcription of target genes and restores apoptosis
- *In vivo* ReACp53 halts progression and shrinks tumors bearing aggregation-prone p53
- p53 aggregation in cancer is a target for therapy with ReACp53 as a lead compound

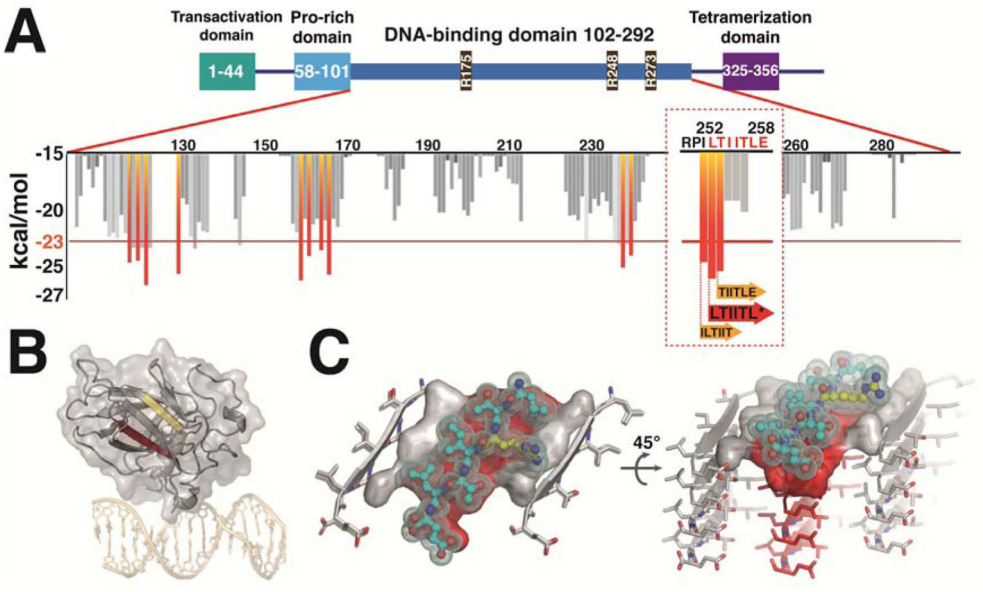

Figure 1. p53 aggregation propensity and ReACp53 docking on the $p53_{252-258}$ amyloid zipper structure

A. ZipperDB (http://services.mbi.ucla.edu/zipperdb/) predicts multiple segments in the p53 DNA-binding domain as aggregation prone. The highest propensity ones are located in the 252-258 region. Colored bars indicate aggregation-prone segments with Rosetta energies below -23 kcal/mol. **B.** The 252-258 segment (red) is mapped on the p53 DNA-binding domain structure. The segment in yellow (residues 213-217) is the epitope recognized by the PAb240 antibody which binds to partially unfolded p53. Both segments are buried in the p53 structure when the protein is fully folded. DNA is in gold. **C.** The ReACp53 peptide (ball-and-stick; cyan, blue and red represent carbon, nitrogen and oxygen atoms respectively) is modeled on the $p53_{252-258}$ amyloid steric zipper structure determined in this study ("PDB: 4RP6"). The arginine in position 3 (in yellow) creates a steric clash with the adjacent β-sheet and additionally impedes incoming molecules from adhering on top while binding to the steric zipper below. Three adjacent β-sheets (in grey and red) of the p53 amyloid spine structure are shown viewed down (left) or nearly perpendicular to the fibril axis (right). See also Tables S1–2 and Figure S1.

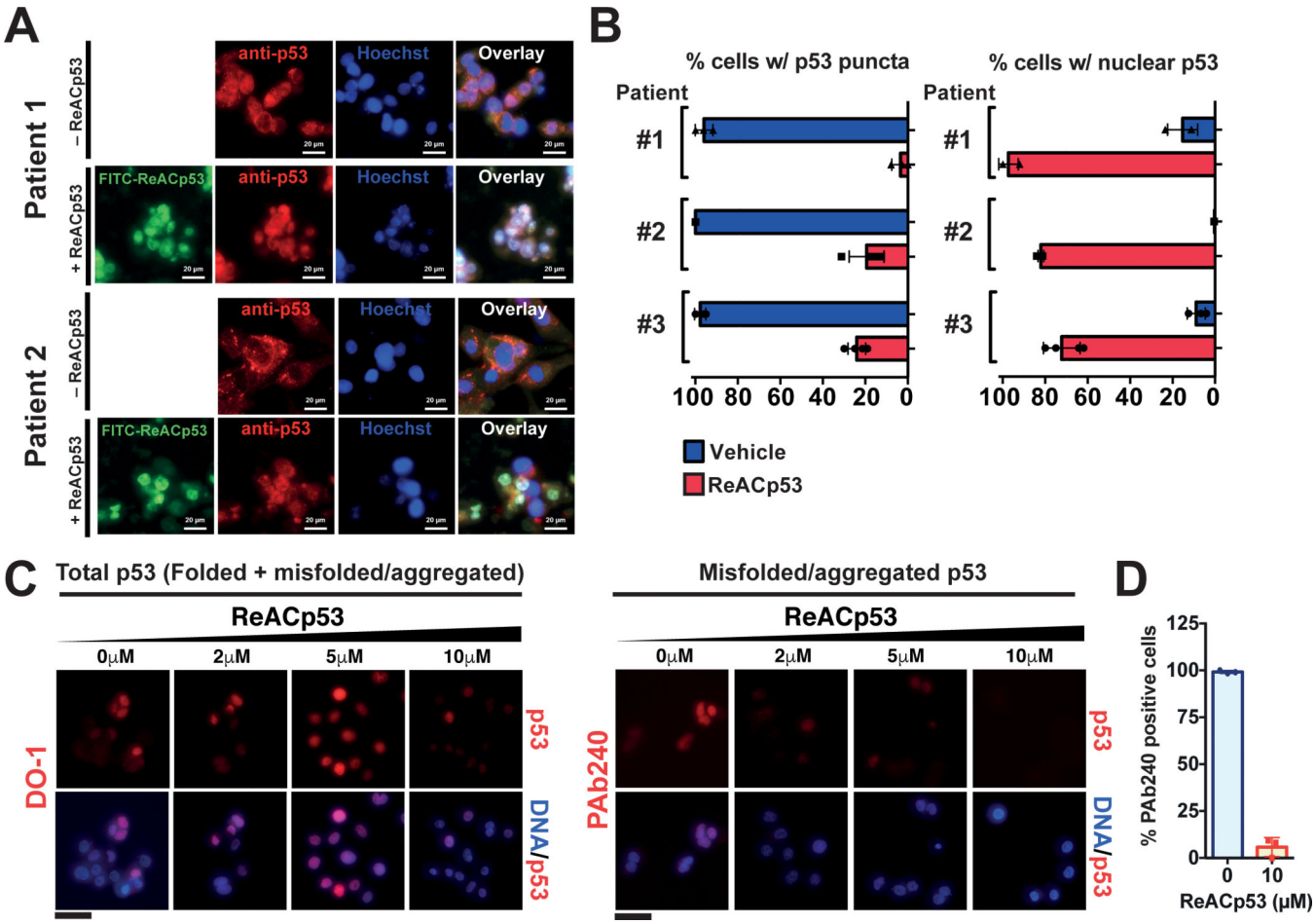

Figure 2. ReACp53 inhibits p53 aggregation in primary cells from HGSOC patients, and re-localizes p53 to the nucleus in an active conformation

A. Mutant p53 forms aggregates appearing as puncta in the cytosol of primary cells from two HGSOC patients (see Figure S2A for additional examples). ReACp53 reduced the number of cells with puncta and caused p53 to localize to the nucleus. Scale bar: 20 μm. **B.** Quantification of number of cells with aggregated p53 and nuclear p53 in three clinical samples. The number of cells with puncta or nuclear p53 counted in 3–5 different fields of view was expressed as % of the total number of cells ± %SD; symbols represent the values for the individual fields of view, bars are average values.**C.** DO-1, an antibody that recognizes p53 regardless of its conformation, binds to p53 in S1 GODL cells over a range of ReACp53 concentrations. PAb240, a conformation-specific antibody that binds only to mutant-like, inactive p53, recognizes and stains p53 in untreated cells, but not in ReACp53-treated cells, indicating that ReACp53 restores p53 to an active conformation. Scale bars: 50 μm. **D.** Quantification of PAb240 staining; the number of positively-stained cells in 3-5 different field of views is expressed as % of the total number of cells ± % SD. Symbols represent % calculated for the individual field of views, bars are average values. See also Tables S3-4 and Figure S2.

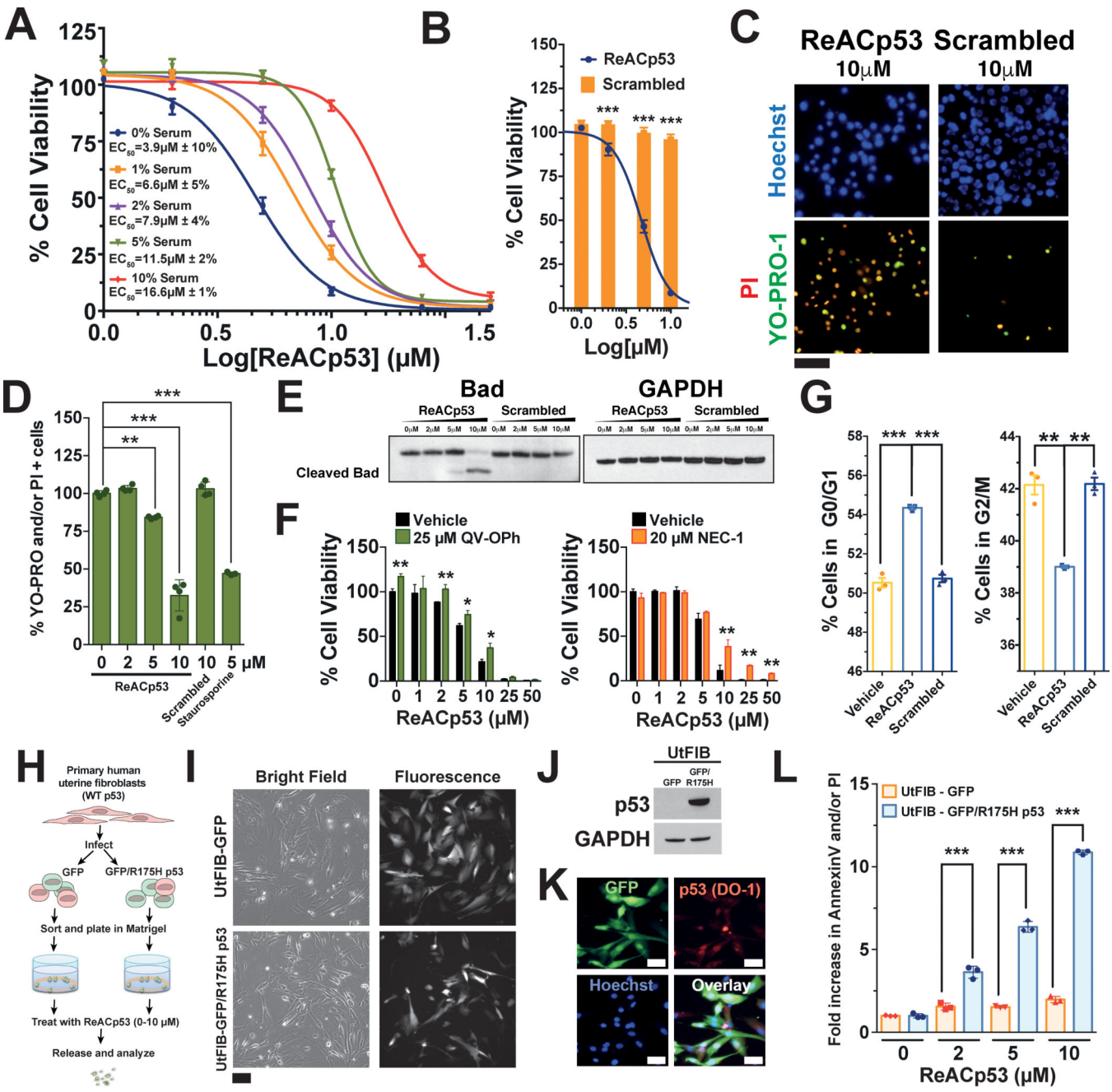

Figure 3. ReACp53 causes cancer cell death

A. MTS assay shows a ReACp53 concentration-dependent decrease in cell viability in S1 GODL cells. Values are represented as the average of 6 independent experiments (n=3/experiment) ± SEM. Average EC_{50} values from all experiments and their coefficient of variation (CV) are reported. **B.** A scrambled control peptide does not exhibit significant effect. ReACp53 is represented as the average of 6 independent experiments (n=3/experiment) ± SEM, Scrambled is presented as average of 3 independent experiments (n=3/experiment) ± SEM. Means were compared with t-tests, ***p<0.0001. **C.** ReACp53-treated OVCAR3 cells stained with YO-PRO-1 and PI to label apoptotic and necrotic cells. A

scrambled peptide control did not elicit significant cell death. Scale bar: 100 μm. **D.** YO-PRO-1/PI stain of S1 GODL cells treated for 16h as quantified by flow cytometry. Scrambled peptide and staurosporine were included as controls. Symbols represent biological replicates (n=2) for two independent experiments, bars show the average for all experiments ± SD. Statistical significance was calculated by performing a repeated measure ANOVA with Holm-Sidak's multiple comparison test, **p<0.001, ***p<0.0001. **E.** Western blot showing Bad cleavage in S1 GODL cell upon treatment with ReACp53 at concentrations of 5 μM and above, indicative of cell death. GAPDH stain was performed on the same membrane after stripping. **F.** MTS assay for ReACp53/QV-OPh or NEC-1 co-treatments. Triplicates for each concentration were measured, one representative experiment out of n=4 (QV-OPh) or n=3 (NEC-1) is shown. ReACp53-induced cell death could be partially rescued by inhibiting apoptosis with QV-OPh (at low ReACp53 concentrations) or with NEC-1 (at high ReACp53 concentrations). Averaged values normalized to vehicle are reported as % ± SD. Means were compared with unpaired two-tailed t tests. *p<0.005, **p<0.0005. **G.** Cell cycle distribution of S1 GODL cells treated with vehicle, 5 μM ReACp53 or 5 μM scrambled peptide for 4/5 hours as evaluated by DNA content measured by flow cytometry. Symbols represent biological replicates (n=2) for two independent experiments, bars show the average for all experiments ± SEM. Statistical significance was calculated by performing a repeated measure ANOVA with Holm-Sidak's multiple comparison test, **p<0.001, ***p<0.0001. **H.** Schematic of the UtFIB infection experiment. **I.** Bright field and green fluorescence of cells post-infection show GFP expression. Scale bar: 100 μm. **J.** Western blot of lysates from GFP- and GFP/R175H p53 infected UtFIB showing p53 expression. GAPDH stain was performed on the same membrane after stripping. **K.** Immunofluorescence of fixed GFP/R175H p53 infected UtFIB showing p53 distribution in the cells. Scale bars: 50 μm **L.** Annexin V/PI staining of GFP- and GFP/R175H p53 infected UtFIB grown in 3D treated for 2 days with ReACp53 as measured by flow cytometry. One representative experiment is shown (n=3). Biological replicates (symbols, n=3) are normalized to vehicle and expressed as fold change ± SD. ANOVA with Tukey HSD significance criterion was performed to calculate p-values. ***p<0.0001. See also Figure S3.

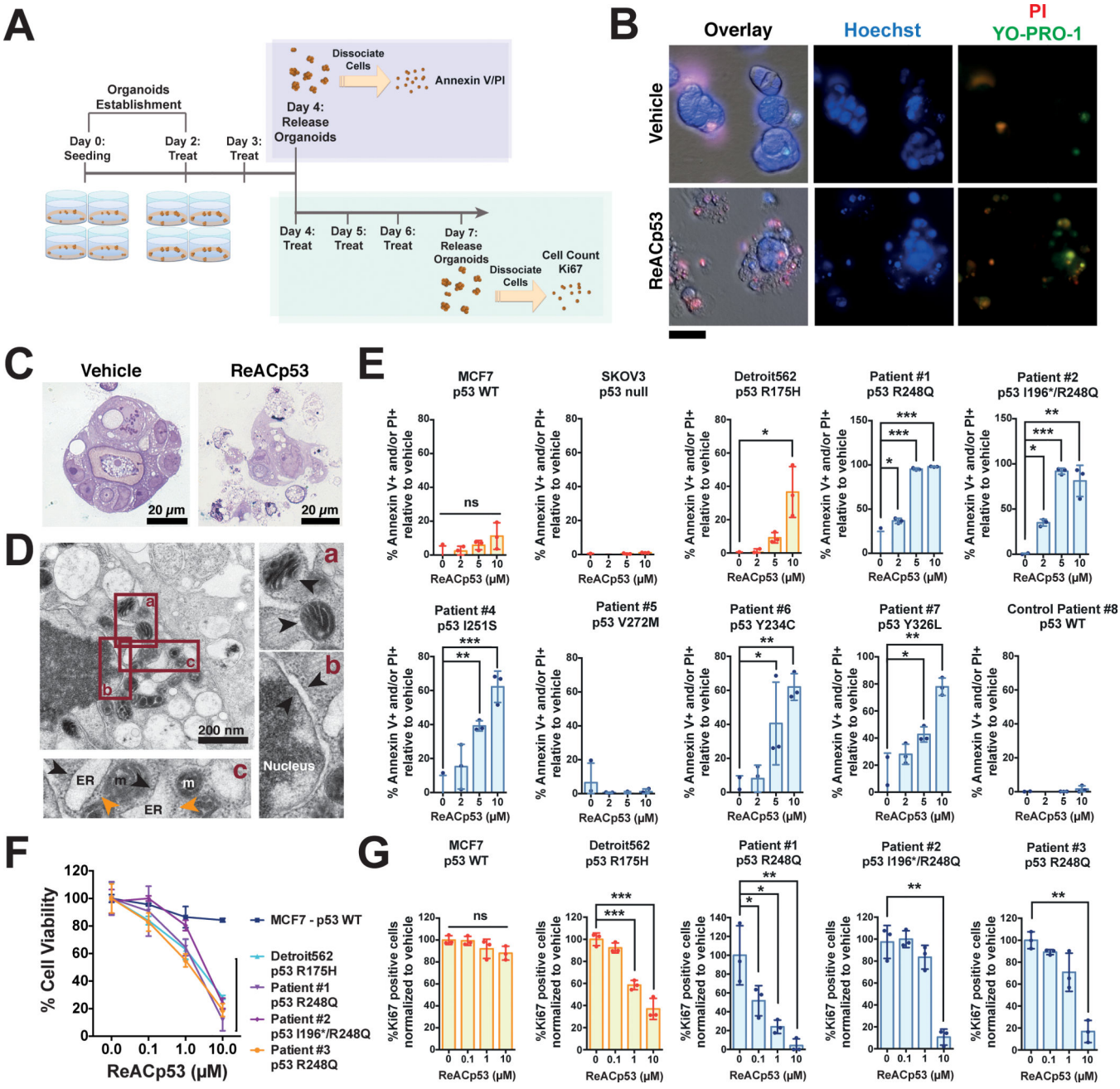

Figure 4. ReACp53 causes cell death in organoids generated from HGSOC samples bearing p53 mutations

A. Schematics of the experiments performed in the 3D organoid model system. The blue and green boxes represent the two different types of experiment performed. **B.** S1 GODL organoids treated with 10 μM ReACp53 undergo a dramatic change in cell morphology and internalization of YO-PRO-1/PI, indicative of cell death. Scale bar: 50 μm. **C.** Semi-thin sections of the spheroids show the catastrophic effect of ReACp53 on spheroid morphology. **D.** TEM analysis of the same sample shows several features of apoptotic cells, including condensed mitochondria (a.), an enlarged nuclear envelope (b.) and enlarged ER (c., black arrowheads) and free ribosomes (orange arrowheads). **E.** ReACp53 affects cell viability of

organoids generated from cell lines or HGSOC primary samples bearing p53 mutations. Organoids were treated for 2 days with the indicated ReACp53 concentrations and Annexin V/PI staining was measured by flow cytometry. Symbols are individual replicates (n=3), bars are average ± SEM; one representative experiment shown (n≥2). p-values were calculated by repeated measure ANOVA with Holm-Sidak's multiple comparison test *p<0.05, **p<0.005, ***p<0.0001. **F.** Cell viability determined after a week of daily ReACp53 treatments by cell counting of triplicate samples. Values are normalized to vehicle; symbols show the average of triplicates ± SD.**G.** ReACp53 induces a significant decline in % of Ki67 positive cells relative to vehicle after a one-week treatment course as quantified by intracellular Ki67 levels measured by flow cytometry. Symbols represents individual replicates, bars average ± SD. Statistics calculated as in E. *p<0.05, **p<0.005, ***p<0.0001. See also Figure S4.

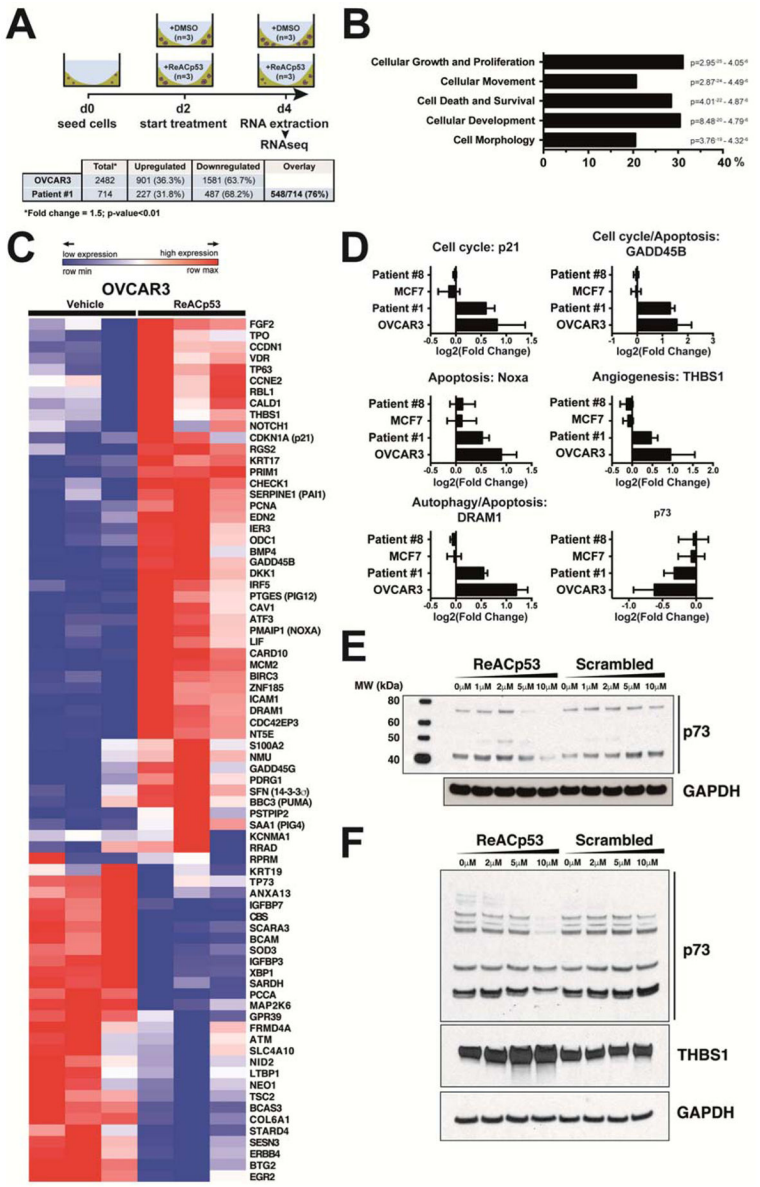

Figure 5. RNAseq of ReACp53 treated organoids

A. Scheme of experimental setup and overview of results. **B.** IPA analysis of molecular functions for the OVCAR3 dataset. **C.** Heat map of a subset of p53 pathway genes differentially regulated in ReACp53-responsive OVCAR3 organoids. Several canonical p53 targets are present. **D.** Fold change for a subset of p53 transcriptional targets. Data are shown as log2(Fold Change), bars represent the average of three replicates ± SD.**E.** OVCAR3 cells have less p73 protein upon ReACp53 exposure as visualized by western blot. **F.** p73 reduction and thrombospondin increase at the protein level in S1 GODL cells correlates with the mRNA levels. In all cases, GAPDH stain was performed on the same membrane after stripping. All blots were repeated three times on three independent cell lysates. One representative example is shown. See also Table S5 and Figure S5.

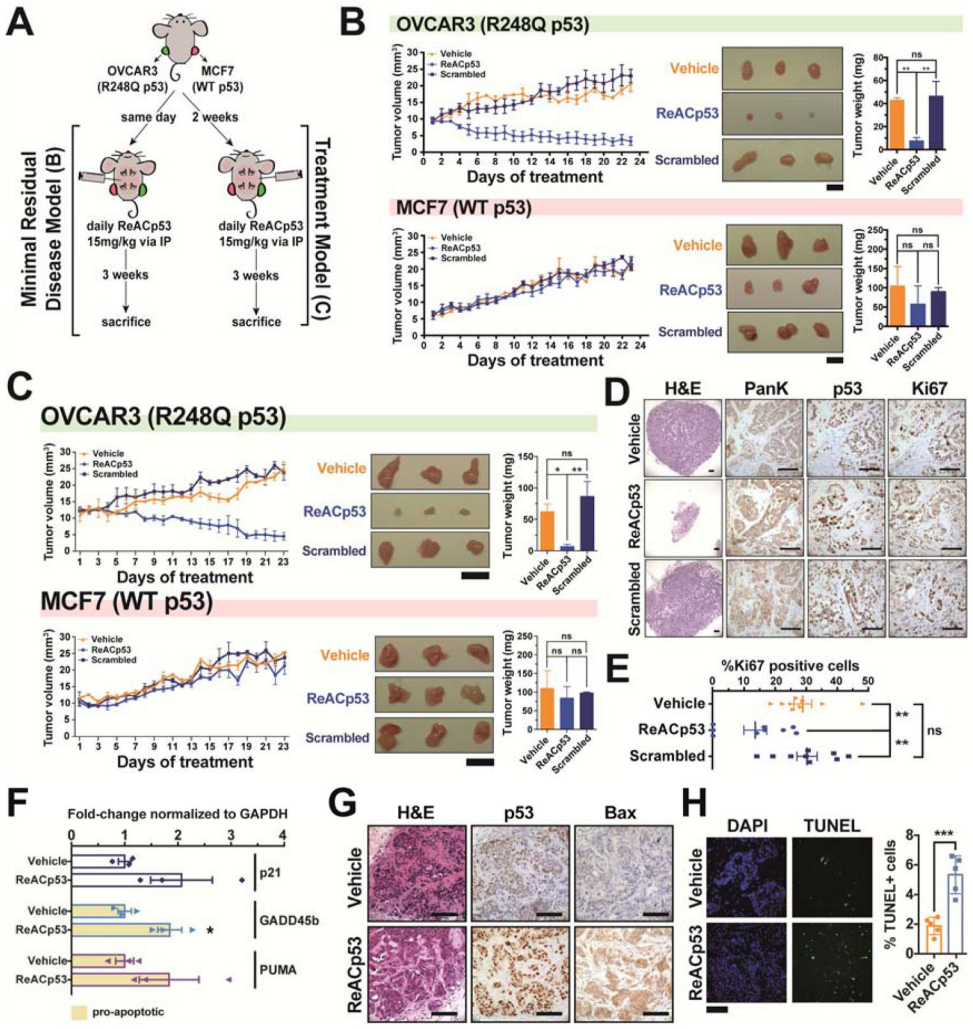

Figure 6. ReACp53 causes regression of xenografts bearing an aggregation-prone p53 mutant *in vivo*

A. Schematics of the experimental design for xenograft models. Both *in vivo* experiments were performed twice, with n=3 mice/group, one representative experiment is shown. **B.** Minimal residual disease model. Tumor growth monitored over time showed a reduction in size of OVCAR3 but not MCF7 xenografts in mice treated with ReACp53. Data are shown as average volumes (symbols, n=3) ± SEM. Means of tumor weights (n=3) are shown as averages (bars) ± SD and compared using an ANOVA model and Tukey HSD significance criterion, **p<0.05. Scale bars: 1 cm. **C–H.** Treatment model. **C.** Same as in B. *p<0.05, **p<0.005. Scale bars: 1 cm. **D.** H&E and IHC on residual xenografts. Sections were stained for PanK, p53 and Ki67. Scale bars: 50 μm. **E.** Total and Ki67-positive cells were quantified on three different fields for each xenograft, and reported as % Ki67 positive cells (symbols). Lines represent the average for each treatment group ± SEM. p-values were calculated by ANOVA using the Tukey HSD significance criterion. **p<0.01. **F.** QPCR analysis of residual S1 GODL xenografts treated with 30 mg/kg ReACp53 for 9 days. Symbols represents the fold-change normalized to GAPDH for n=3 xenografts, bars are average values ± SEM. *p<0.05. **G.** H&E and IHC this short-term treated xenografts shows

abundant Bax expression, indicative of apoptosis. Scale bar: 100 μm. **H.** TUNEL assay also showed a significantly higher proportion of death cells in ReACp53-treated grafts. Symbols represent the % of TUNEL-positive cells in five field of view sampling all the tumors while bars show the average values ± SD, ***p<0.0001. Scale bar: 100 μm. See also Table S6 and Figure S6.

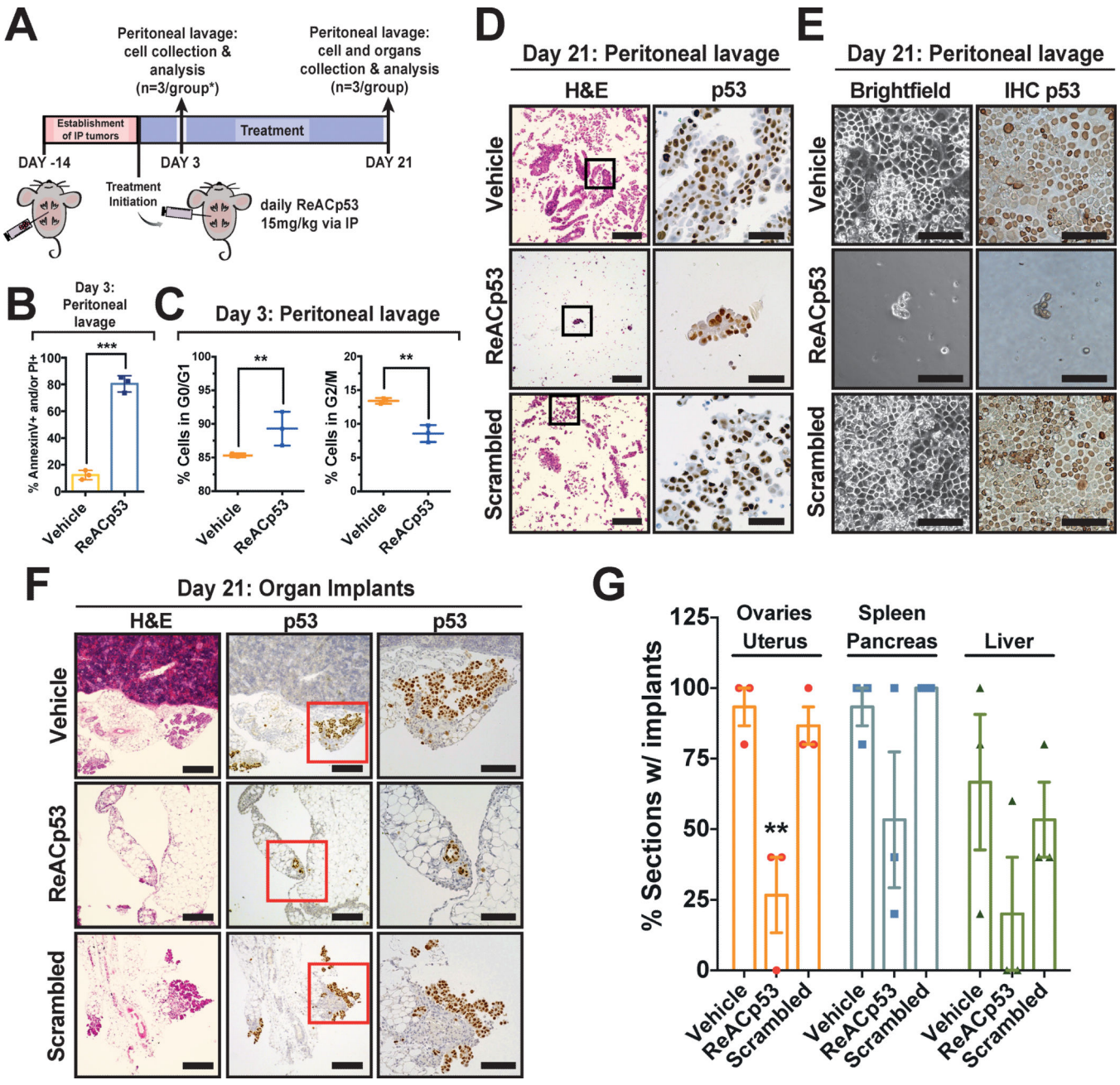

Figure 7. ReACp53 causes regression of intraperitonal disseminated tumors *in vivo*

A. Schematics of the IP disseminated disease model experiment. **B.** Viability of cancer cells obtained from ascites (discussed in Methods) after 4 daily treatments as measured by flow cytometry of Annexin V/PI stained cells. Symbol represent values from individual mice (n=3/group), bars are average ± SD. Means were compared by t test. ***p<0.001 **C.** Cell cycle distribution of tumor cells obtained from ascites as measured by flow cytometry. Symbol represent values from individual mice (n=3/group), lines are average ± SD. Means were compared by t test. **p<0.01. **D.** Analysis of pelleted ascites-derived cancer cells by H&E and IHC. The black boxed area is magnified on the right. Scale bars: 200 μm for H&E; 50 μm for IHC. **E.** Bright field and IHC of cancer cells obtained from ascites after a three-

week treatment and plated to confirm viability. Quadruplicates were pleated for each mouse (n=3 mice/group). The ReACp53-treated samples did not yield any live and proliferating cell. Scale bars: 100 μm. **F.** Organ implants as visualized by H&E and identified by positive p53 IHC staining. Scale bars: 200 μm for H&E and low magnification IHC; 50 μm for high magnification IHC.**G.** Quantification of organ implants upon histological examination of p53 stained sections. This conservative analysis does not take into account implant size, which were typically small (3–5 cells) in ReACp53 treated samples. Each symbol represents the average for all sampled sections (n=5) for a given mouse; three mice are reported. Bars represent averages for the three mice ± SEM. A statistically significant difference in the presence of implants in the uterus/ovaries was detected by performing repeated measure ANOVA with Holm-Sidak's multiple comparison test. **$p<0.05$. Scale bars: 200 μm for H&E; 50 μm for IHC.

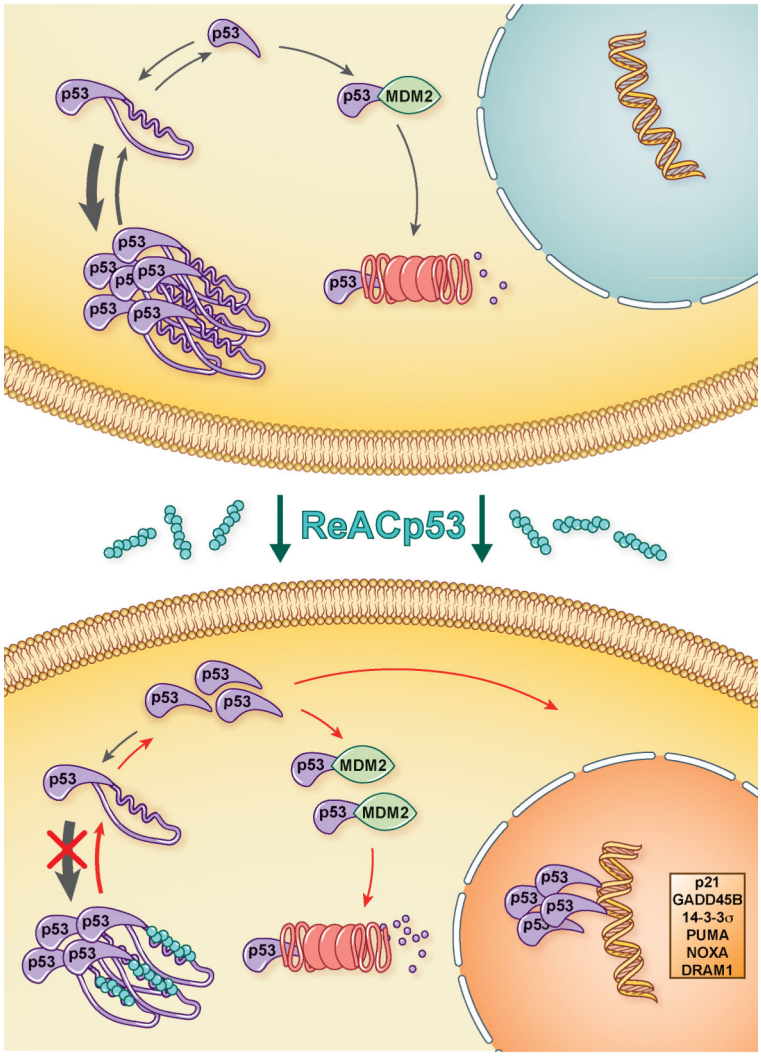

Figure 8. Model for the mechanism of action of ReACp53 (cyan)

Unstable p53 mutants partially unfold, exposing the aggregation prone segment LTIITLE. This segment interacts with the same segment from other p53 molecules, driving p53 into its inactive aggregated state (top). ReACp53 treatment blocks the aggregation pathway, shifting the equilibrium towards functional, soluble p53 (bottom). Functional p53 enters the nucleus and induces cell death and proliferation arrest. Folded p53 interacts with MDM2 and is degraded.